Michigan State University

National Superconducting Cyclotron Laboratory

NEUTRON HALOS IN THE Na ISOTOPES

B.A. BROWN and W.A. RICHTER

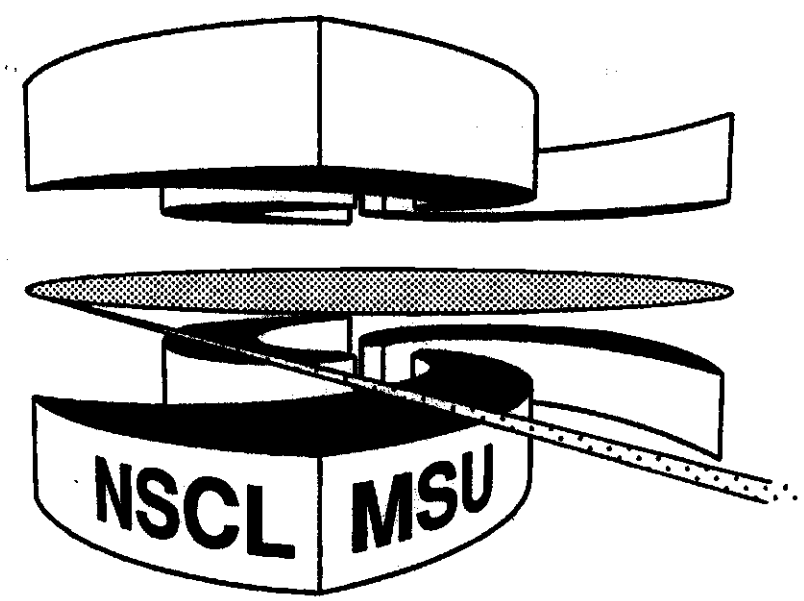

MSUCL-1016 **MARCH 1996**

Neutron halos in the Na isotopes

B.A. Brown* and W.A. Richter+

* *Department of Physics and Astronomy and National Superconducting Cyclotron Laboratory, Michigan State* **University,** *East Lansing, Michigan 48824*

+ *Department of* **Physics,** *University of Stellenbosch, Stellenbosch 7600, South Africa*

Abstract

The neutron and proton density distributions of the Na isotopes out to the proton and neutron drip lines are calculated in the spherical Hartree-Fock model with a wide variety of density-dependent Skyrme interactions. The results are compared to recent experimental data for the interaction cross sections and for the rms radii. We discuss the role of the deformed intruder states and the problems associated with predicting the location of the neutron drip line for this mass region.

I. INTRODUCTION

Recent experimental results have been reported for the matter radii of the neutron-rich Na isotopes based upon a Glauber-model analysis of interaction cross-section data [1]. Comparison of these results with estimates of the charge radii [2] provides one of the best examples of neutron skin behaviour for an extended series of isotopes. It also brings back into interest the long standing observation of the vanishing of the N=20 shell closure for ^{32}Mg and nearby nuclei. The theoretical comparison made in [1] was only to a relativistic mean-field (RMF) calculation. The purpose of this paper is to put the comparisons on a broader basis of the non-relativistic Skyrme interaction as well as to highlight some of the

special shell-model features of the most neutron-rich Na isotopes which are important for determining the location of the drip line.

Spherical and deformed Skyrme HF calculations for the Na isotopes were first carried out many years ago [3]. Although our results have some similarities to the early deformed calculations, we want to explore the sensitivity to the various Skyrme parameterizations. We carry out spherical calculations which are meant to be complementary to configuration mixed shell-model calculations such as those reported in [4]. Deformation and the vanishing of the N=20 shell closure in ^{32}Mg and in nearby nuclei are a result of this configuration mixing.

II. RESULTS AND DISCUSSION

We start out with the SGII Skyrme interaction [5]. This interaction has been used previously both for global charge radii comparisons [6] as well as for the neutron halos of light nuclei [7]. Later we will explore the full range of Skyrme parameterizations. The neutron rms radii obtained with SGII are compared with the experimental range of values deduced in [1] in Fig. 1. The limits given in Table I of ref. [1], were based on two extreme assumptions: (a) $R_n(^A\mathrm{Na}) = r_0 N^{1/3}$ and $R_p(^A\mathrm{Na}) = R_n(^{23}\mathrm{Na}) = 3.137$ fm, and (b) $d_p(^A\mathrm{Na}) = d_n(^A\mathrm{Na}) = 0.564$ fm (the value for ^{23}Na), where R_k is the half-density radius, and d_k is the diffuseness in the Fermi-type distribution

$$\rho_k(r) = \frac{\rho_k(0)}{1 + \exp[(\mathrm{r} - \mathrm{R_k})/\mathrm{d_k}]}$$

assumed for both protons and neutrons. It is expected that the true values would lie between these extremes. The experimental results shown in Fig. 1 with error bars were obtained under the assumptions (a) and (b), and are indicated as filled circles and open squares, respectively. The solid line is the SGII HF results obtained when the spherical orbitals are occupied sequentially in the order given by the HF potential, namely: $0d_{5/2}$, $1s_{1/2}$, $0d_{3/2}$, $0f_{7/2}$, $1p_{3/2}$ and $1p_{1/2}$. (For the closed-shell configurations such as N=20, these calculations

correspond directly to the exact HF equations. For the open-shell configuration the potential is approximated by the spherical potential obtained by weighting the radial density profile for a given orbital by its occupation probability.) At $N = 34$ the next orbital, $0f_{5/2}$, is unbound and the drip line is reached. For the sd-shell nuclei ($N = 9 - 20$) we also show the SGII HF results (crosses) obtained with the fractional orbital occupancies calculated from the Brown-Wildenthal sd-shell wave functions [8]. The SGII HF results are close to the RMF calculation shown in [1] up to $N = 15$, but for $N = 16 - 19$ the RMF values lie somewhat higher than our calculation and also outside the experimental errors. The experimental dip around $N = 11$ is not explained by either calculation.

The results for the proton rms radii are also shown in Fig. 1. Both the RMF and present calculations are in reasonable agreement with experiment. It is remarkable how little the proton radii change compared to the increasing neutron radii, so that by $N = 21$ a significant neutron skin appears. The calculated density profiles and radial density probabilities for the even-N Na isotopes are shown in Figs. 2a and 2b for protons and neutrons, respectively. The neutron density profile shows a large jump in the interior between $N = 14$ and $N = 16$ due to the filling of the $1s_{1/2}$ orbital. These profiles are not well fitted by the Fermi-shape assumed in [1]. However, the neutron density radial profile shows a steady increase between $r = 2.5$ fm and $r = 5.0$ fm, and this part is probably well modeled by the Fermi-shape assumed in the Glauber analysis. One should also keep in mind, as emphasized by Huber et al. [2], that the charge radii (shown in Fig. 1) have some uncertainty owing to the unknown contribution from the specific-mass shift. Thus even though it is interesting to compare our results for the proton and neutron radii separately, it is probably more meaningful to compare directly with the matter radii obtained from [1], by using our densities to calculate the Glauber-model cross sections, as was done for light nuclei in [7]. The results with the zero-range interaction are shown in Fig. 3. The calculations are in excellent agreement with experiment. It is interesting to note the change in calculated slope at the semi-magic numbers $N = 14$ and $N = 28$, with the change at $N = 14$ also appearing in the data. Changes in the experimental charge-radii differences also appear at $N = 14$ and $N = 28$ [6].

The rather large neutron skin for the neutron-rich Na isotopes is in contrast to the situation near the line of maximum stability for nuclei such as ^{208}Pb [9,10], where the proton and neutron radii are nearly equal even when N/Z is relatively large. So it may be coincidental that a specific Skyrme interaction whose parameters are designed to reproduce the properties of nuclei near stability works so well in a very different situation. To examine how robust the predictions are, we have calculated the neutron and proton radii for ^{31}Na with many of the Skyrme parameterizations which have been proposed up to now. The symbols used in the literature to denote the various Skyrme interactions used [5,11–17] are given in Table 1. As shown in Fig. 4, all parameterizations give about the same result – the large difference between the proton and neutron radii is indeed a very robust feature of the Skyrme parameterization. The experimental value for the proton rms radius and the limits for the neutron rms radius are also shown, as well as the values of the relativistic mean field calculation [1].

Since the potential well for protons is determined mainly by the neutron density, the proton potential becomes larger in radius as a function of increasing neutron number, and thus one may think that the proton radius should also increase. However, the potential for protons also becomes deeper as a function of increasing neutron number and this tends to counteract the effect of the radial size increase. The difference between the proton and neutron potentials manifests itself in a difference between the Fermi energies for protons and neutrons (as observed in the proton and neutron separation energies). In ^{31}Na the Fermi energy for protons is about 12 MeV larger than that for neutrons, in contrast to the situation in a nucleus such as ^{208}Pb where the proton and neutron Fermi energies are about equal to each other. The situation for ^{48}Ca is intermediate to that of ^{31}Na and ^{208}Pb with a proton-neutron rms radius difference of 0.1 – 0.2 fm [18,19] and 6 MeV difference in the Fermi energies.

The spherical HF calculations for $N = 20$ presented in Fig. 1 have a closed sd-shell configuration. However, it has long been known experimentally that the $N = 20$ is not a good closed shell for ^{32}Mg and nearby nuclei. This information comes from the binding

energy systematics [20,21], the low-lying 2^+ energy in ^{32}Mg [22] and from the beta decay [23]. The increase in the Na proton radii between $N = 15$ and $N = 20$ may be another indication of the deformation at $N = 20$. Theoretically, this deformation has been understood from deformed HF calculations [3] and well as configuration mixed shell-model calculations [4,24,25]. The shell-model approach provides the most detail in terms of excited state energies and wave functions. The shell-model calculation for ^{31}Na of [4] indicates that the $2\hbar\omega$ intruder configuration with two neutrons excited from the sd to the fp shell lies lower in energy than the closed sd shell configuration. It appears from the shell-model calculations that the intruder states are isolated to a region around ^{32}Mg and for this reason it has been referred to as an "island of inversion". A similar inversion for the ground state ^{11}Be ground state is well known and can also be understood from shell-model calculations [26].

We assume that beyond a neutron number of $N = 23$ that the configurations become spherical again, and that it thus makes sense to use the ordering of level occupancies obtained in the spherical Hartree-Fock calculations. But this has yet to be confirmed experimentally.

To take into account the effect of the intruder states on the rms radii we repeated the SGII HF calculation for ^{31}Na with orbital occupancies corresponding to the $2\hbar\omega$ excitation. Radii calculated with the HF densities modified so that two neutrons are excited from the $0d_{3/2}$ orbital to the $0f_{7/2}$ orbital differ very little from the closed-shell radii. However, due to core-polarization, the deformation and associated radius change is usually larger than obtained in the valence shell-model calculations. The experimental value of $\beta = 0.51$ for the proton deformation in ^{32}Mg [27] would lead $[< r^2 >=< r^2 >_o (1 + \frac{5\beta^2}{4\pi})]$ to a 5 % or 0.15 fm increase in the proton rms radius and a similar increase for the neutron rms radius. The experimental proton rms radii for the Na isotopes [2] (shown in Fig. 1) are consistent with an increase of about this magnitude, but as mentioned above, a quantitative interpretation is difficult owing to the uncertainty in the specific-mass shift contributions.

The spherical calculations are continued in Figs. 1 and 3 out to the drip line. The proton radii remain relatively flat and the neutron radii (and the interaction cross sections) increase more rapidly as the $N = 34$ drip line is reached. The more rapid increase corresponds to the

change from the filling of the $0f_{7/2}$ orbital to the 1p orbitals which have a smaller angular momentum barrier and smaller separation energies and thus a large rms radius.

The position of the neutron drip line is primarily determined by the valence neutron single-particle energies (SPE). The SGII neutron SPE for the most neutron-rich Na isotopes are shown in Fig. 5. One observes an overall decrease in their energy, but when $N = 34$ is reached the next orbital, $0f_{5/2}$, is unbound and thus $N = 35$ is not stable. What is important in Fig. 5 are the absolute neutron SPE at $N = 20$ and their slope as a function of neutron number. We first discuss the absolute energies.

Are the SPE obtained with the SGII interaction correct or appropriate for the Na isotopes? We cannot compare the calculation with the experimental binding energies at $N = 20$ because of the deformation effect discussed above. The nearest "spherical" nucleus available for comparison is ^{34}Si. When $N = 20$ is a closed shell, it is appropriate to equate $\epsilon_h =$ BE($N = 19$) – BE($N = 20$) with the $0d_{3/2}$ (hole) SPE, and $\epsilon_p =$ BE($N = 20$) – BE($N = 21$) with the $0f_{7/2}$ (particle) SPE, where BE is the experimental binding energy. The experimental binding energy differences for ^{34}Si are compared in Fig. 6 with the results of all of the Skyrme parameterizations. Here we see some variation with respect to the various interactions. SGII (number 11) does well on the difference $\epsilon_p - \epsilon_h$, but misses the absolute value by about 2 MeV.

The binding energy differences also include some correlation energies (mainly due to like-particle pairing and proton-neutron $Q \cdot Q$ interactions) beyond the monopole interaction which determines the single-particle energies. The sd-pf shell-model calculation [4] gives -0.85 MeV for the non-monopole correlation energy which would make the empirical ^{34}Si $0f_{7/2}$ SPE about -1.62 MeV compared to the SGII value of -4.14 MeV. Indeed, the SGII interaction systematically underbinds the valence particle states in light nuclei; for example, the ^{16}O $0d_{5/2}$ experimental (SGII) SPE is -4.14 (-7.05) MeV and the ^{40}Ca $0f_{7/2}$ SPE is -8.36 (-9.70) MeV. Thus, we must assume that the SPE for the neutron-rich Na isotopes obtained with SGII are also too bound by about 2.5 MeV. Qualitatively this would shift all of the points in Fig. 5 up by about this amount. This means that all of the Na isotopes are

on the very edge of being bound and that the non-monpole correlation energies as well as the intruder states energies will be the determining factor in the location of the drip line.

Assuming an $N = 20$ closed shell, the shell-model result [4] for the ^{32}Na energy minus the ^{31}Na energy is -0.56 MeV. This energy difference can be decomposed into $+1.12$ MeV coming from the (unbound) monopole $0f_{7/2}$ SPE plus -1.67 MeV correlation energy. When the intruder states are included, the ground state of ^{31}Na has a two-particle two-hole $(2p-2h)$ configuration (Fig. 4 of [4]), the ground state of ^{32}Na has a $2p-1h$ configuration (Fig. 5 of [4]), and the energy difference is -1.14 MeV. The experimental value [29] is $-2.4(5)$ MeV. Again, assuming an $N = 20$ closed shell, the shell-model result for the ^{33}Na energy minus the ^{31}Na energy is -4.1 MeV which can be approximately decomposed into $+2.2$ MeV from the SPE, -3.9 MeV from neutron-neutron pairing and -2.4 MeV from the proton-neutron correlations. The experimental value [29] is $-3.3(15)$ MeV. (The calculated change due to intruder states is small.) Thus the correlation energy calculations will be important for determinig the properties of all neutron-rich Na isotopes, but they are beyond the scope of the present work. Similar comments apply to the Ne isotopes, where we note that ^{32}Ne [30] and ^{31}Ne [31] are both stable, but the masses have not yet been measured.

The other qualitative feature which is important for the location of the drip line is the downward slope of the SPE and the subsequent binding of higher single-particle orbitals as a function of increasing neutron number, as seen in Fig. 5. Is the slope seen in Fig. 5 characteristic of all Skyrme interactions? The slope changes very slowly with Z and thus we can address this question by looking at the results of the Z=14 calculations. We show in Fig. 7 the difference between the $f_{7/2}$ SPE in ^{42}Si ($N = 28$) and ^{34}Si ($N = 20$). Although some of the older Skyrme interactions have a wide range of slopes, the results for SGII (number 11) and the more recent parameterizations (numbers 12-20) show less variation. The question as to whether or not the Skyrme parameterizations are applicable to the most neutron-rich nuclei remains to be tested experimentally.

As a final illustration of the effects of intruder states in ^{32}Mg and nearby nuclei, we show in Fig. 8 the $N = 20$ shell gap as given by the difference between the SGII $0f_{7/2}$ SPE and

the $0d_{3/2}$ SPE as a function of Z (crosses). These are compared to the values obtained from the experimental binding energy difference BE(N = 19) + B(N = 21) - 2 BE(N = 20) (circles). Between ^{34}Si (Z=14) and ^{40}Ca (Z=20) the agreement is good. But below Z=14 the agreement quickly becomes worse with the experimental gap becoming small compared to the spherical calculation and indicating a change in structure away from a closed shell for $N = 20$ to an open-shell intruder state.

III. CONCLUSION

We have calculated the rms radii, density distribitions and single-particle binding energies for Na isotopes using spherical HF calculations with Skyrme interactions. A comparison of measured rms radii up to $A = 32$ with the calculated values based on the Skyrme SGII interaction indicates good general agreement, and the rapidly increasing neutron skin thickness as a function of A is substantiated by the calculation. The calculated Glauber model cross sections are also in excellent agreement with the data. The systematics of the single-particle binding energies using various parameterizations of the Skyrme interactions have been studied in the vicinity of the neutron drip line. Since the valence single-particle states for the neutron-rich Na isotopes ($N > 20$) are on the edge of being bound, the stability and the location of the drip line will strongly depend upon the correlation energies.

ACKNOWLEDGMENTS

W. R. would like to acknowledge the hospitality and support of the National Superconducting Cyclotron Laboratory, Michigan State University. Our research was partly supported by the National Science Foundation grant PHY94-03666. We thank Gregers Hansen for his helpful comments on a draft of this paper.

REFERENCES

[1] T. Suzuki, H. Geissel, O. Bochkarev, L. Chulkov, M. Golovkov, D. Hirata, H. Irnich, Z. Janas, H. Keller, T. Kobayashi, G. Kraus, G. Münzenberg, S. Neumaier, F. Nickel, A. Ozawa, A. Piechaczeck, E. Roeckl, W. Schwab, K. Sümmerer, K. Yoshida, and I. Tanihata, Phys. Rev. Lett. 75, 3241 (1995)

[2] G. Huber, F. Touchard, S. Büttgenbach, C. Thibault, R. Klapisch, H. T. Duong, S. Liberman, J. Pinard, J.L. Vialle, P. Juncar, and P. Jacquinot, Phys. Rev. C18, 2342 (1978).

[3] X. Campi, H. Flocard, A. K. Kerman and S. Koonin, Nucl. Phys. A251, 193 (1975).

[4] E. K. Warburton, J. A. Becker and B. A. Brown, Phys. Rev. C41, 1147 (1990).

[5] N. van Giai and H. Sagawa, Nucl. Phys. A371, 1 (1981), N. van Giai and H. Sagawa, Phys. Lett. B106, 379 (1981)

[6] B. A. Brown, C. R. Bronk and P. E. Hodgson, J. Phys. G10, 1683 (1984).

[7] G. F. Bertsch, B. A. Brown and H. Sagawa, Phys. Rev. C39, 1154 (1989).

[8] B. A. Brown and B. H. Wildenthal, Annu. Rev. Nucl. Sci. 38, 29 (1988).

[9] B. A. Brown, S. E. Massen, J. I. Escudero, P. E. Hodgson, G. Maduga and J. Vinas, J. Phys. G9, 423 (1983).

[10] C. J. Batty, E. Friedman, H. J. Gils and H. Rebel, Adv. Nucl. Phys. 19, 1 (1989).

[11] D. Vautherin and D. M. Brink, Phys. Rev. C5, 626 (1972)

[12] M. Beiner, H. Flocard, N. van Giai, Nucl. Phys. A238, 29 (1975)

[13] H.S. Kohler, Nucl. Phys. A257, 301 (1976)

[14] J. Treiner and H. Krivine, J. Phys. G2, 285 (1976)

[15] H. Krivine, J. Treiner, O. Bohigas, Nucl. Phys. A336, 155 (1980)

[16] J. Bartel, P. Quentin, M. Brack, C.Guet, and M. B. Hakansson, Nucl. Phys. A386, 79 (1982)

[17] J. Friedrich and P.G. Reinhard, Phys. Rev. C33, 335 (1986)

[18] B. A. Brown, S. E. Massen and P. E. Hodgson, J. Phys. 5, 1655 (1979).

[19] W. R. Gibbs and J. P. Dedonder, Phys. Rev. C46, 1825 (1992).

[20] C. Thibault, R. Klapisch, C. Rigaud, A. M. Poskanzer, R. Prieels, L. Lessard and W. Reisdorf, Phys. Rev. C12, 644 (1975).

[21] B. H. Wildenthal and W. Chung, Phys. Rev. C22, 2260 (1980).

[22] C. Detraz, D. Guillemaud, G. Huber, R. Klapisch, M. Langevin, F. Naulin, C. Thibault, L. C. Carraz and F. Touchard, Phys. Rev. C19, 164 (1979).

[23] B. H. Wildenthal, M. S. Curtin and B. A. Brown, Phys. Rev. C28, 1343 (1983).

[24] A. Poves and J. Retamosa, Phys. Lett. B184, 311 (1987); Nucl. Phys. A571, 221 (1994).

[25] N. Fukunishi, T. Otsuka and T. Sebe, Phys. Lett. B296, 279 (1992).

[26] H. Esbensen, B. A. Brown and H. Sagawa, Phys. Rev. C51, 1274 (1995)

[27] T. Motobayashi et al., Phys. Lett. B346, 9 (1995).

[28] Fauerbach et al., to be published in Phys. Rev. C.

[29] G. Audi and A. H. Wapstra, Nucl. Phys. A595, 409 (1995).

[30] D. Guillemaud-Mueller et al., Phys. Rev. C41, 937 (1990).

[31] I. Tanihata, private communication.

FIGURES

FIG. 1. Calculated and measured proton and neutron rms radii as a function of neutron number of the Na isotopes. The calculations were based on the SGII Skyrme parameterization. The small dots and solid line correspond to the HF calculation with simple occupation numbers, and the crosses were obtained with the sd-shell occupation numbers. The solid points in the top panel are the experimental proton rms radii. The points with error bars in middle and bottom panels correspond to the experimental neutron rms radii obtained with assumptions (a) and (b), respectively, from [1].

FIG. 2. The calculated density profiles $\rho(r)$ and radial density probabilities $4\pi r^2\rho(4)$ for the even-N Na isotopes obtained with the SGII interaction. The results for protons and neutrons are shown in (a) and (b), respectively. The neutron numbers for some of the lines are indicated.

FIG. 3. Calculated Glauber interaction cross sections obtained with the zero-range interaction of [7] (solid line) compared with the experimental data [1] (filled circles with error bars).

FIG. 4. Calculated proton and neutron rms radii of ^{31}Na for different parameterizations of Skyrme interactions. The experimental and RMF values from Ref. [1] are shown for comparison.

FIG. 5. Single-particle energies (SPE) of the Na isotopes as a function of neutron number, using the SGII Skyrme parameterization. A cross indicates the order in which the orbital are occupied as a function of neutron number.

FIG. 6. Single-particle energies (SPE) of ^{34}Si for different parameterizations of Skyrme interactions. The gaps in the $p_{3/2}$ SPE correspond to unbound cases. The two horizontal lines in the diagram are the $d_{3/2}$ and $f_{7/2}$ values deduced from the experimental binding energies of ^{33}Si, ^{34}Si and ^{35}Si

FIG. 7. Difference between the $f_{7/2}$ SPE in ^{42}Si ($N = 28$) and ^{34}Si ($N = 20$) for the various Skyrme interactions.

FIG. 8. Difference between the $f_{7/2}$ SPE and the $d_{3/2}$ SPE for the $N = 20$ nuclei as a function of Z. The SGII calculation (crosses) is compared with the experimental [29] binding energy difference BE($N = 19$) + B($N = 21$) - 2 BE($N = 20$) (circles).

TABLES

TABLE I. Skyrme interactions used in this paper

Present number	Literature symbol	Reference
1-2	SK1-2	[11]
3-6	SK3-6	[12]
7	SKA	[13]
8	SKB	[13]
9	SKTK	[14]
10	SGI	[5]
11	SGII	[5]
12	M	[15]
13	M*	[16]
14	E	[17]
15	E_σ	[17]
16	Z	[17]
17	Z_σ	[17]
18	Z^*_σ	[17]
19	R_σ	[17]
20	G_σ	[17]

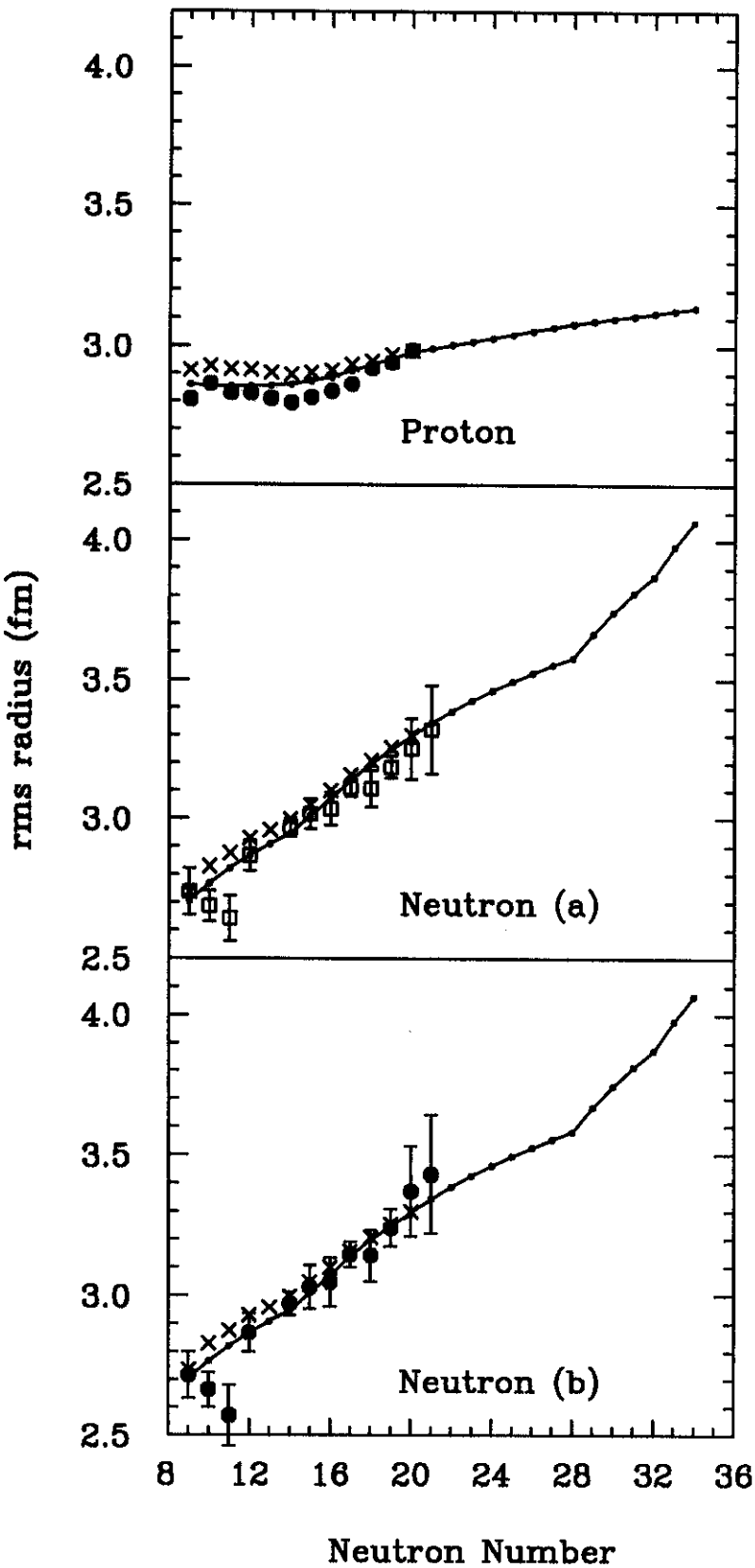
4.0
3.5
3.0
2.5
Proton
4.0
3.5
3.0
2.5
Neutron (a)
4.0
3.5
3.0
2.5
Neutron (b)
rms radius (fm)
8
12
16
20
24
28
32
36
Neutron Number

Figure 1

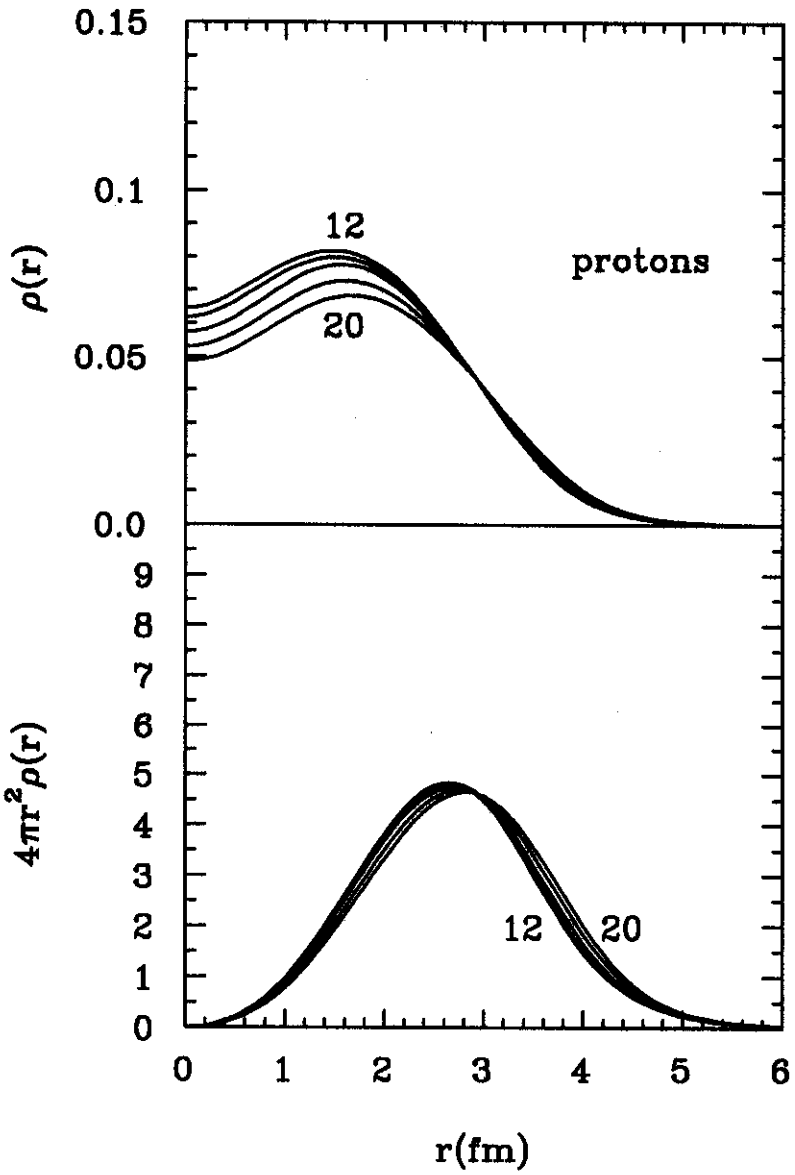
0.15
0.1
0.05
0.0
ρ(r)
12
20
protons
9
8
7
6
5
4
3
2
1
0
4πr²ρ(r)
12
20
0
1
2
3
4
5
6
r(fm)

Figure 2a

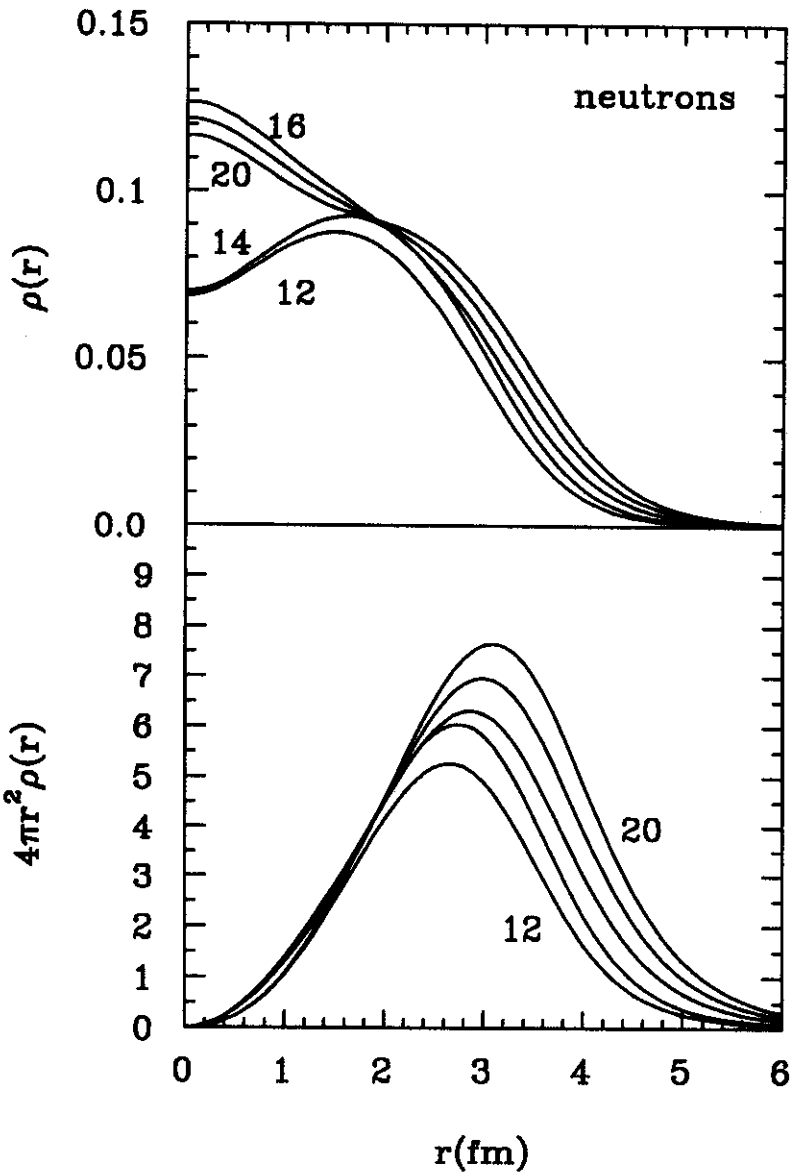
0.15
0.1
0.05
0.0
ρ(r)
neutrons
16
20
14
12
9
8
7
6
5
4
3
2
1
0
4πr²ρ(r)
20
12
0
1
2
3
4
5
6
r(fm)

Figure 2b

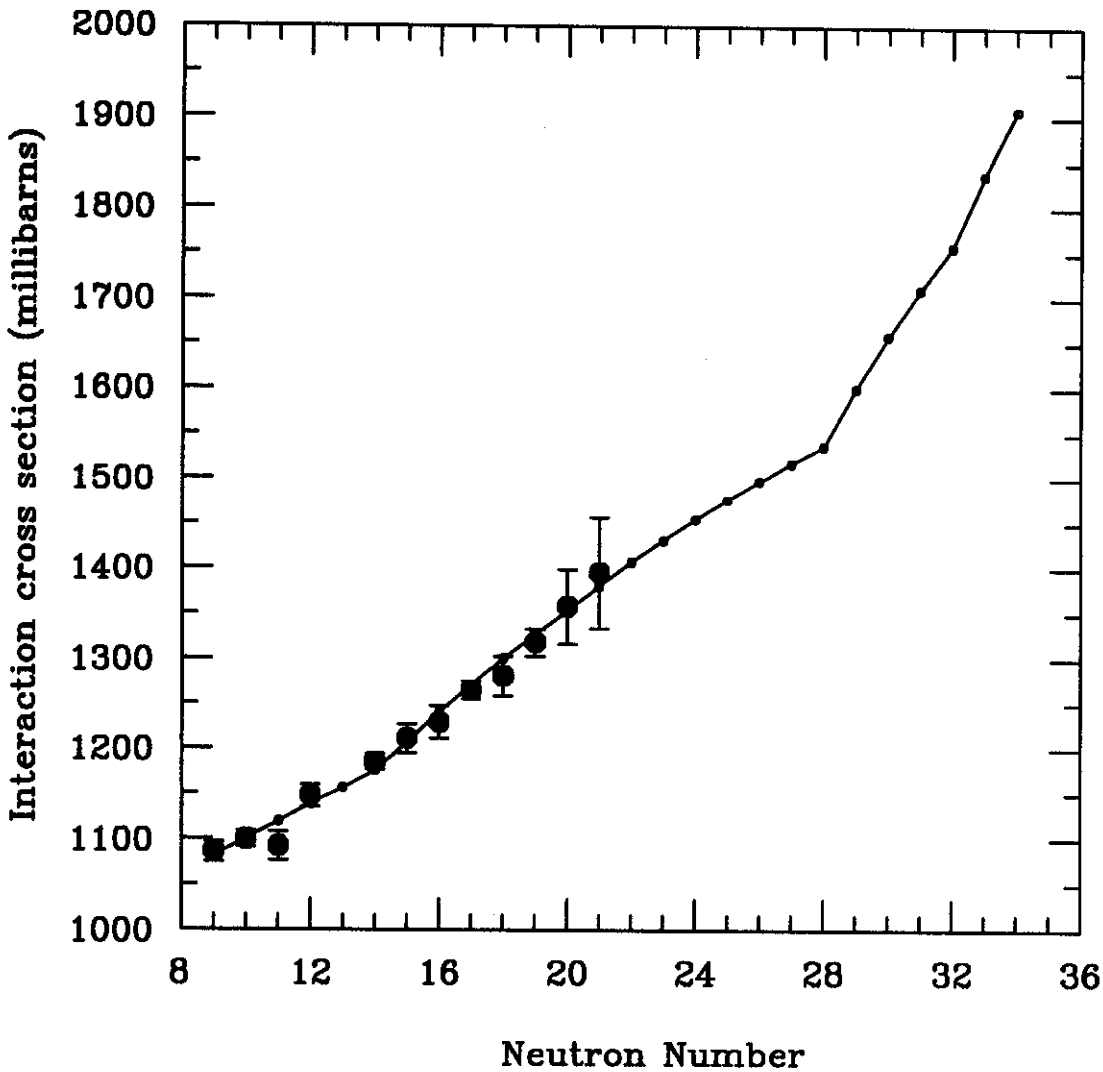
Interaction cross section (millibarns)
2000
1900
1800
1700
1600
1500
1400
1300
1200
1100
1000
8
12
16
20
24
28
32
36
Neutron Number

Figure 3

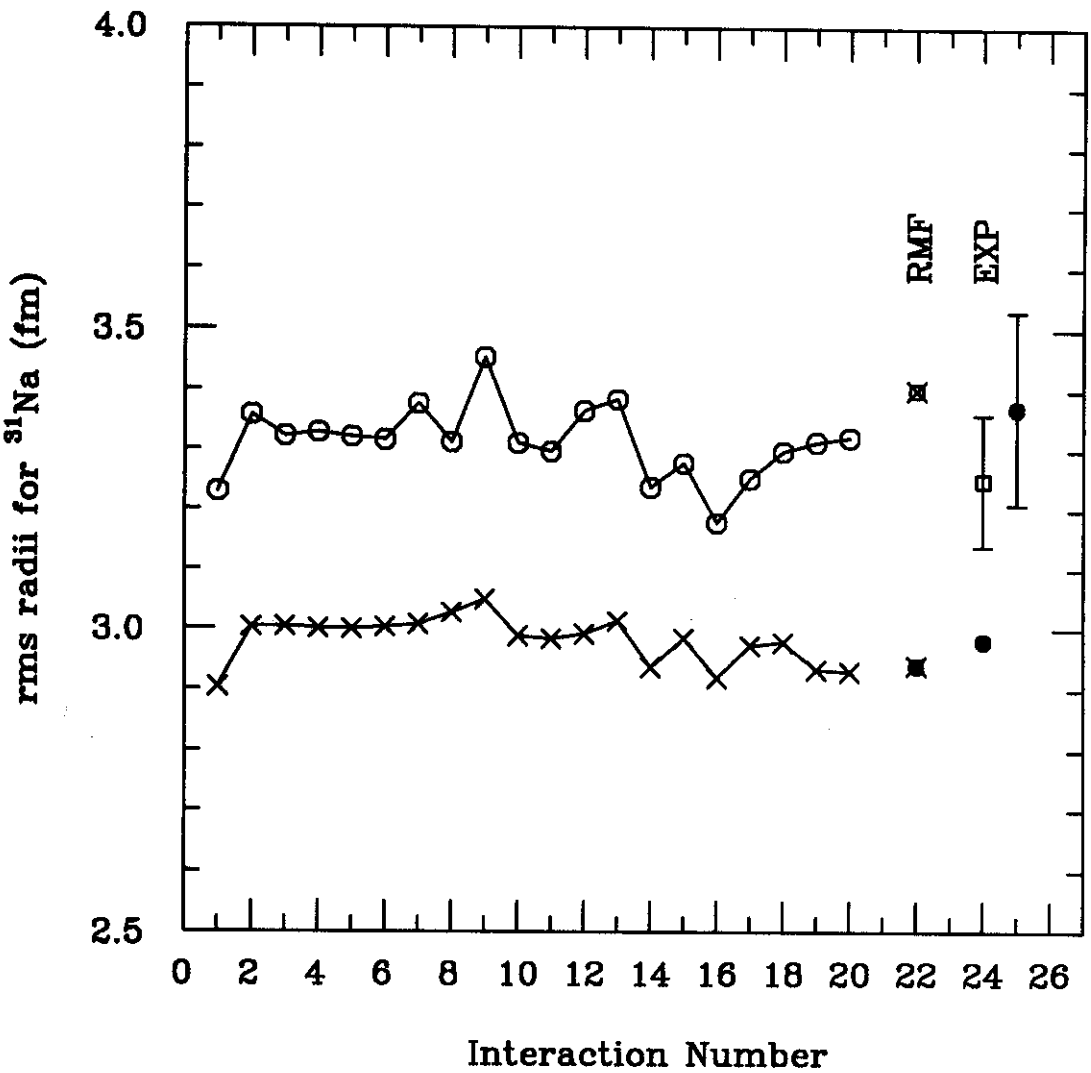
4.0
3.5
3.0
2.5
rms radii for ^{31}Na (fm)
0
2
4
6
8
10
12
14
16
18
20
22
24
26
Interaction Number
RMF
EXP

Figure 4

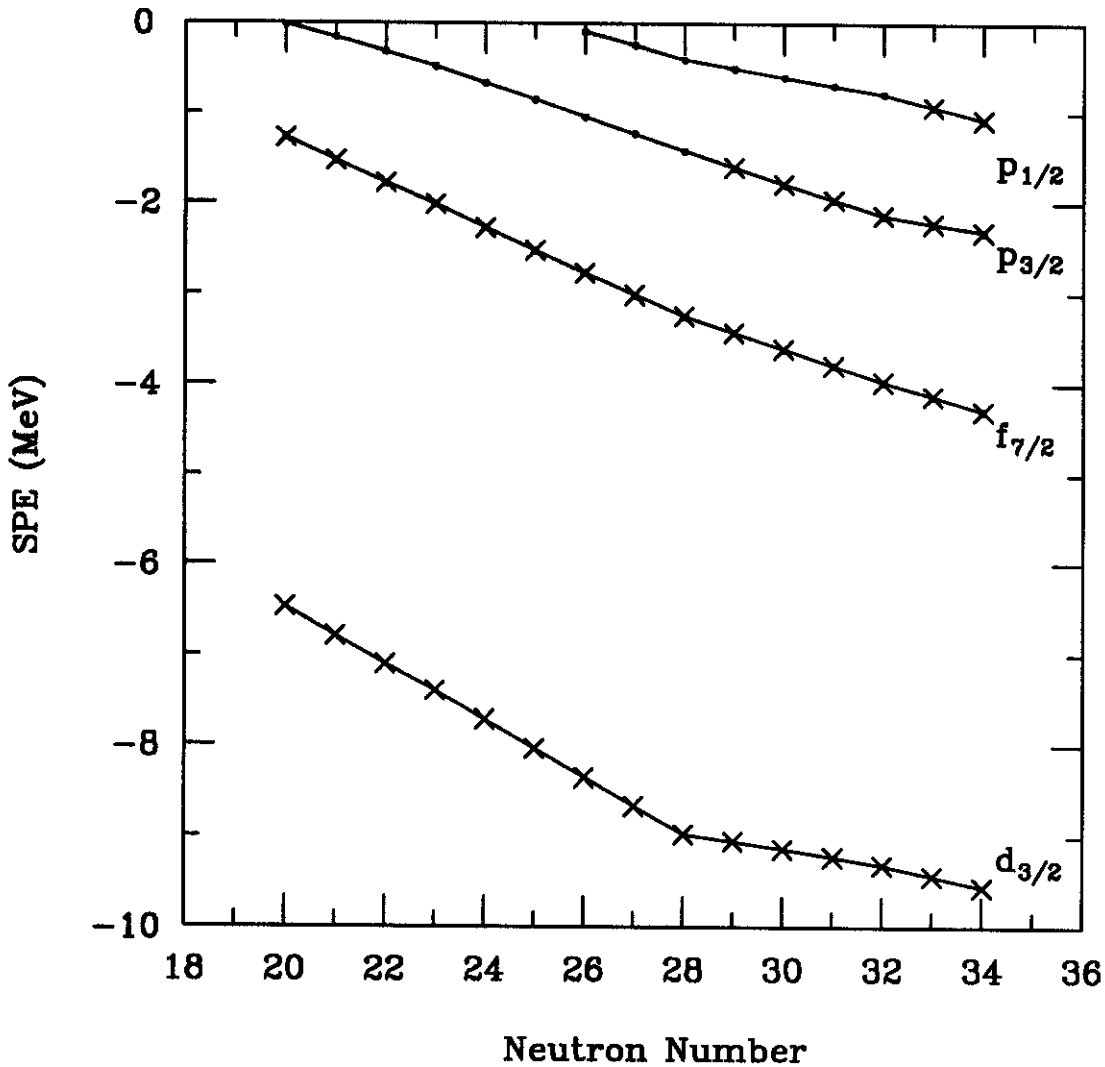
0
−2
−4
−6
−8
−10
SPE (MeV)
18
20
22
24
26
28
30
32
34
36
Neutron Number
p1/2
p3/2
f7/2
d3/2

Figure 5

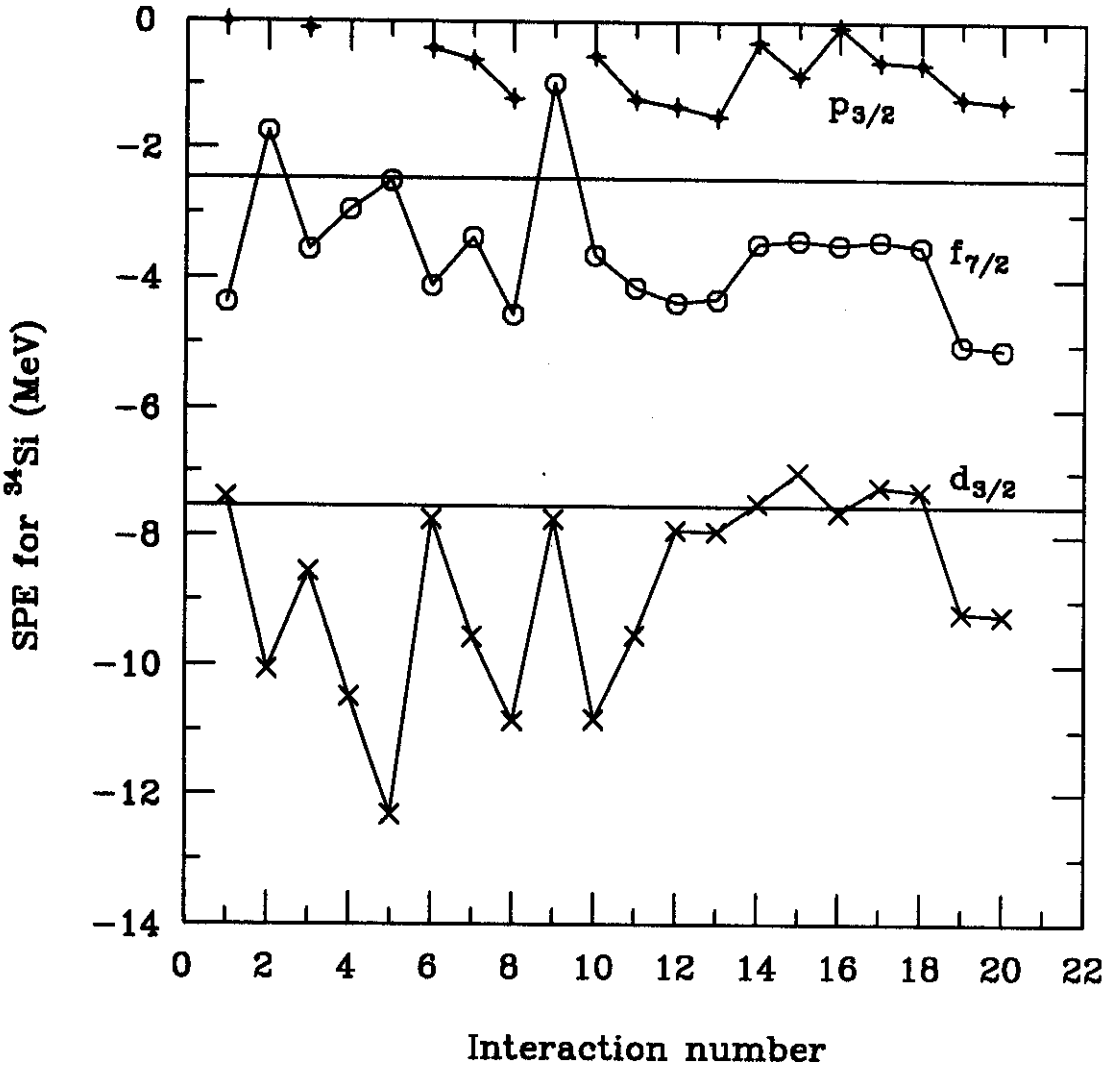
0
−2
−4
−6
−8
−10
−12
−14
0
2
4
6
8
10
12
14
16
18
20
22
SPE for ^{34}Si (MeV)
Interaction number
$p_{3/2}$
$f_{7/2}$
$d_{3/2}$

Figure 6

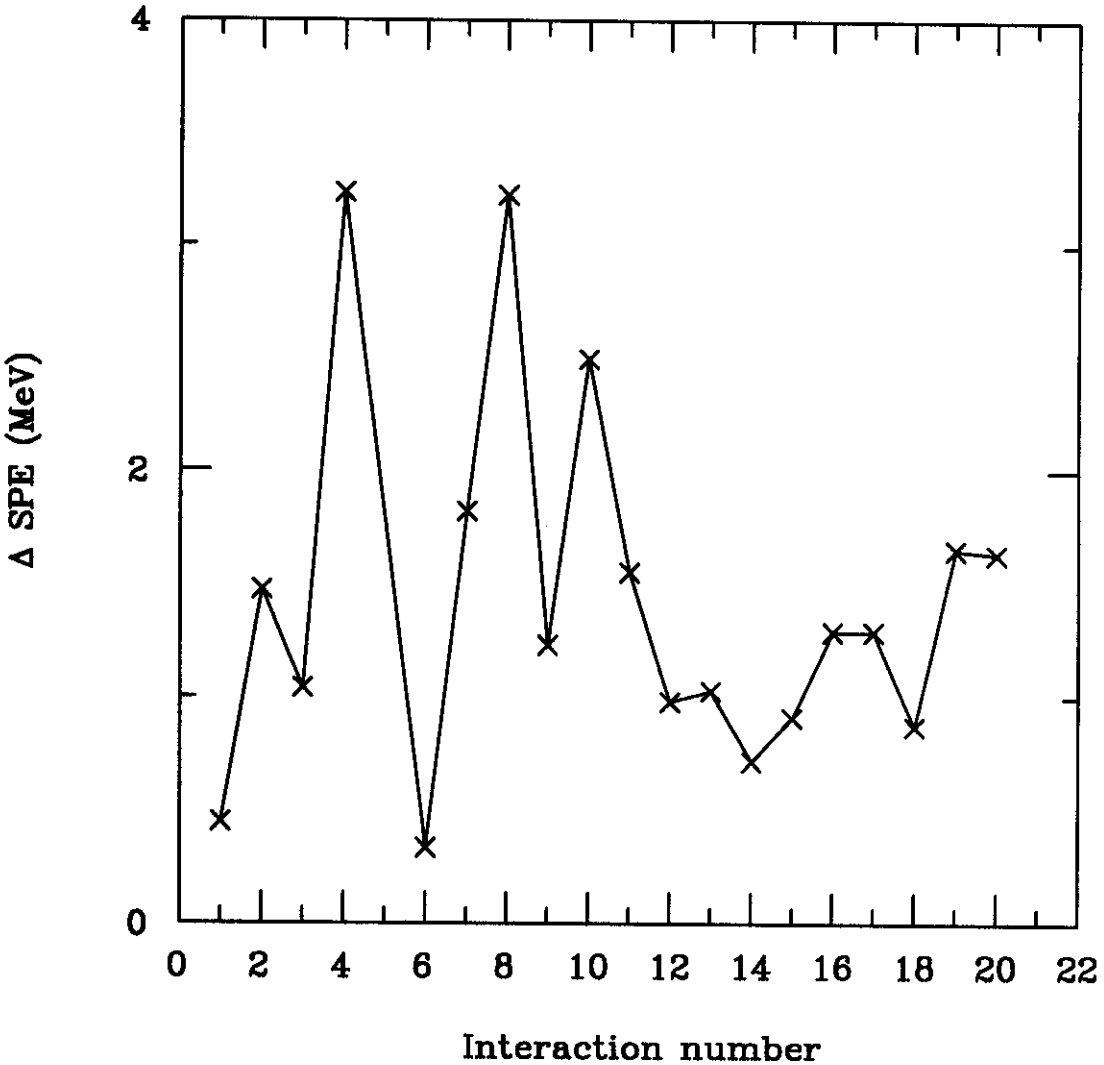

Figure 7

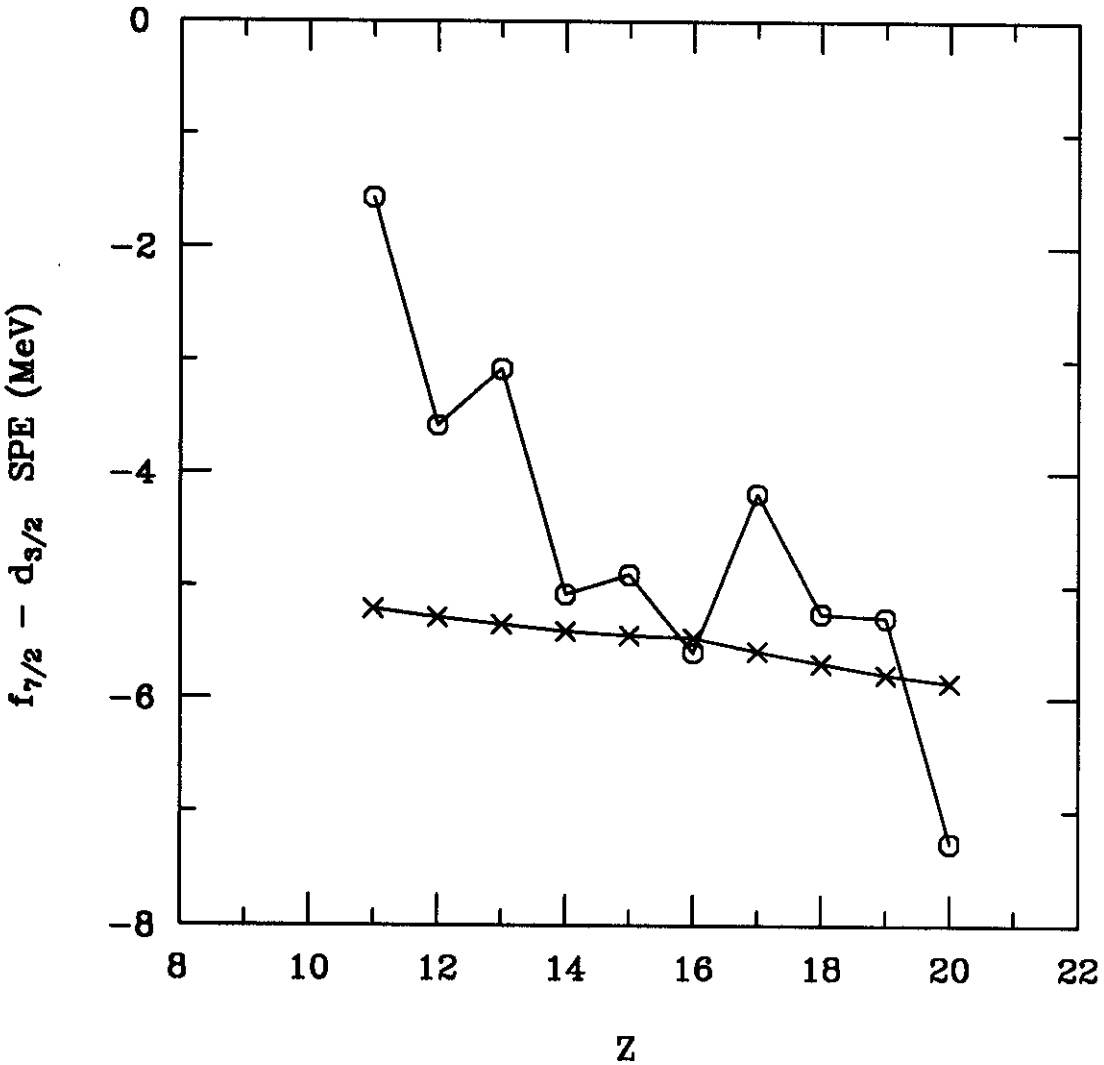

Figure 8